ORIGINAL ARTICLE

SUV_{95th} as a reliable alternative to SUV_{max} for determining renal uptake in 68Ga-PSMA PET/CT

[1,2] Serena Baiocco

[3] Federica Matteucci

[4] Emilio Mezzenga

[3] Paola Caroli

[5] Valentina Di Iorio

[6] Corrado Cittanti

[1,7] Alessandro Bevilacqua

[3] Giovanni Paganelli

[4] Anna Sarnelli

[1] Advanced Research Center for Electronic Systems (ARCES), University of Bologna, Bologna, Italy

[2] Department of Electrical, Electronic and Information Engineering “Guglielmo Marconi” (DEI), University of Bologna, Bologna, Italy

[3] Nuclear Medicine Unit, Istituto Scientifico Romagnolo per lo Studio e la Cura dei Tumori (IRST) IRCCS, Meldola, Italy

[4] Medical Physics Unit, Istituto Scientifico Romagnolo per lo Studio e la Cura dei Tumori (IRST) IRCCS, Meldola, Italy

[5] Oncology Pharmacy, Istituto Scientifico Romagnolo per lo Studio e la Cura dei Tumori (IRST) IRCCS, Meldola, Italy

[6] Diagnostic Imaging Unit - Morphology, Surgery and Experimental Medicine Department, University of Ferrara, Ferrara, Italy

[7] Department of Computer Science and Engineering (DISI), University of Bologna, Bologna, Italy

Corresponding author:

Prof. Alessandro Bevilacqua
ARCES, Via Toffano 2/2, Bologna 40125, Italy
Email: alessandro.bevilacqua@unibo.it

Abstract

Purpose: Widely used in clinical practice, the maximum standardized uptake value (SUV_{max}) is a statistical index highly prone to physical and biological variations, which can lead to unpredictable errors. This study has a methodological aim: to identify a more robust SUV-based index representing the tracer accumulation. In particular, the new metric was tested to confirm the potential of mannitol to reduce renal uptake [68Ga] prostate-specific membrane antigen (^{68}Ga-PSMA).

Procedures: To this aim, our previously published work, proving the efficacy of mannitol, was considered as a background study. Renal SUV_{max} was calculated in nine patients undergoing ^{68}Ga-PSMA positron emission tomography/computed tomography (^{68}Ga-PSMA-PET/CT) at baseline (b-PET/CT) and at follow-up after intravenous infusion of 500 ml of 10% mannitol (m-PET/CT). SUV values of kidney volumes were extracted by a new 3D segmentation method. A new parameter, the median computed on the upper 10% of the SUV distribution (SUV_{95th}), was introduced to better characterize the tracer accumulation. A comparison between SUV_{max} and SUV_{95th} was also performed. Kruskal-Wallis test was used to assess the statistical significance of the differences in SUV_{95th} between b-PET/CT and m-PET/CT.

Results: SUV_{95th} not only confirmed the efficacy of mannitol as demonstrated in the previous study but improved the separability of b-PET/CT and m-PET/CT examinations, overturning SUV_{max} findings in two cases. The outcomes of the Kruskal-Wallis test computed for each kidney proved that differences between b-PET/CT and m-PET/CT SUV_{95th} values were significant (p-value <0.001).

Conclusions: Our findings indicate that SUV_{95th} is a more robust index to assess high uptake level, representing a reliable alternative to SUV_{max}. Independently from the segmentation method, the superiority of SUV_{95th} and its easy computation could make its clinical impact decisive. The results obtained with SUV_{95th}, more representative of tracer

uptake than those with SUV_{max} suggest, in our opinion, that mannitol infusion could be used to reduce the adsorbed dose to the kidneys during ^{68}Ga-PSMA-PET/CT and 177Lu or 225Ac therapy. Our future goal will be confirming this effect in a larger cohort of patients, also verifying the role of SUV_{95th} in the evaluation of tumour response to therapy.

Keywords: PET/CT; SUV_{max}; Reliability; Prostate cancer; Mannitol; PSMA; Standardized Uptake Value; Quantitative imaging

Introduction

Prostate cancer (PC) is the leading cancer in men and the third cause of cancer death worldwide [1]. The diagnostic capacity of conventional imaging modalities such as computed tomography (CT), magnetic resonance imaging and bone scintigraphy for metastasis screening has proven limited for the detection of locoregional and distant metastases in PC patients [2]. Recently, [68Ga] prostate-specific membrane antigen positron emission tomography/computed tomography (^{68}Ga-PSMA-PET/CT) has emerged as a promising diagnostic tool for PC patients [3]. Indeed, the new radiotracer ^{68}Ga-PSMA has shown great theranostic potential [4], with an excellent diagnostic performance for primary and secondary staging thanks to its ability to detect PSMA expression, even at low levels of serum prostate-specific antigen (PSA) [2].

Despite the benefits of using ^{68}Ga-PSMA-PET, several studies have shown that PSMA is physiologically expressed by the lacrimal and salivary glands, intestines and kidneys [1]. In the kidneys, PSMA is expressed in the apical epithelium of proximal tubuli [5]. Osmotic diuretics of the proximal tubuli, such as mannitol, facilitate water excretion whilst inhibiting the reabsorption of sodium, chloride, and other solutes.

The potential use of mannitol to reduce ^{68}Ga-PSMA kidney uptake has already been proven in a study by our group [6] in which we analyzed the maximum standardized uptake values (SUV_{max}). The results were subsequently confirmed in a dosimetric study of patients treated with 177Lu-PSMA [7]. However, SUV_{max} represents the activity of very few or even just one pixel (*i.e.* that having the maximum intensity value). Thus, it is not representative of the high activity concentration of the structure considered as a whole.

Despite the widespread use of SUV_{max}, its application to compare baseline and follow-up examinations is problematic given that changes in SUV_{max} are often statistical fluctuations, rather than real changes in radiotracer uptake. With this in mind, we re-analyzed ^{68}Ga-PSMA-PET/CT baseline and follow-up examinations, considering the distribution of SUV values to look for a more robust statistical index that can better represent the tracer

accumulation. Accordingly, SUV distribution values were derived using a new 3D kidney segmentation method.

Materials and methods

Patient Enrolment

Nine patients with PC were considered for this study (age 71±5 years, range 64-78). All patients were treated with radical prostatectomy for intermediate-/high-risk (pathological Gleason score 7-9) disease and referred for ^{68}Ga-PSMA-PET/CT imaging following biochemical recurrence. Mean PSA levels at the time of the image acquisition were 2.25±0.96 [0.89-3.21] ng/mL. According to our clinical protocol [6], patients underwent baseline ^{68}Ga-PSMA-PET/CT (b-PET/CT) to localize the site of relapse; those with a negative b-PET/CT and PSA progression during follow-up underwent a second ^{68}Ga-PSMA-PET/CT with concomitant intravenous infusion of 10% mannitol (m-PET/CT). Two different protocols were used for the mannitol infusion, as previously reported [6]:

- 500 mL of mannitol infused over 40 minutes immediately after the injection of ^{68}Ga-PSMA (A-infusion);
- 250 mL of mannitol infused over 15 minutes immediately before and again after ^{68}Ga-PSMA injection (B-infusion).

A-infusion was used for the first 3 patients and B-infusion for the subsequent 6 patients. The mean injected activity of ^{68}Ga-PSMA was (173±19) MBq.

Image Acquisition

^{68}Ga-PSMA-PET/CT images were acquired with Biograph mCT Flow PET/CT system (Siemens Healthineers, Erlangen, Germany) 60 minutes after intravenous injection of ^{68}Ga-PSMA. All patients were asked to void before the scan was initiated. An unenhanced CT scan (120 kV, 80 mA/s) was acquired before the PET series. PET data were corrected

for decay, random and scatter events. Attenuation correction was performed using the low-dose CT component of the study.

Image Analysis

The distribution of all kidney SUV values was used to identify a more robust SUV-based parameter to represent high uptake. To this purpose, a 3D segmentation method was implemented using ImageJ software (v1.47 or later) [8], Java3D plugin collection and Java 1.6 or later. As shown in Fig. 1, the procedure was divided into 3 phases: pre-processing, processing and post-processing.

Fig. 1 Flowchart of the computer-assisted 3D kidney segmentation.
ROI, region of interest

The pre-processing phase involved the manual delimitation of the structure (in this case, kidneys) to be segmented in only one of the slices composing it, *e.g.* by drawing a circle around it, as shown in Fig. 2 (a) and (b).

Fig.2 Example of kidney segmentation (a). The procedure starts with manually outlining the kidney (b) and the selection of the window/level (W/L). The resulting image (c) is used for the object detection (d). The last step involves the filling of the object detected (e).
ROI, region of interest

This procedure enabled us to create a local histogram of the structure being analyzed, facilitating the subsequent processing steps.

The processing phase started with the selection of an appropriate window/level (W/L). W/Ls were automatically set to enhance the kidneys, as seen in Fig. 2 (c).

Blob (or structure) detection was performed using the 3D Object Counter plugin embedded with a threshold-based segmentation method [9]. Segmentation results were

visualized through the 3D ROI Manager plugin [10], permitting us to further identify and extract the objects of interest, in this specific application the kidneys that appeared as hollow organs (Fig. 2(d) and Fig. 3).

Fig. 3 3D visualization of the kidneys. Regions with lower uptake such as the renal pelvis were almost discarded during the processing phase. To facilitate subsequent analysis and 3D measurements, results of the object detection were post-processed through in-house developed ImageJ Macro software.

The post-processing phase involved the filling of the objects detected (Fig. 2 (e)) and for this purpose an ImageJ macro was developed to fill and integrate the regions of interest (ROIs) of the structure. In this way, it was possible to obtain the total kidney volume, including the regions characterized by lower uptake such as the renal pelvis, not included in the previous steps. The output of the macro was the entire set of ROIs of the structure, which will be used for subsequent analyses and 3D measurements, such as the extraction of SUV values from the volumes.

Once kidney SUV distributions relating to each scan had been derived, the Tukey method [11] was used to identify possible outliers in SUV distributions (p-value<0.05). As expected, these distributions often present outliers and are the highest SUV values, implying that in many cases SUV_{max}, despite representing just one or few pixels, statistically also represents a distribution outlier. For this reason, the last decile of the SUV value distribution, corresponding to the upper tail and including statistically representative high values, was considered so as to characterize a high uptake level in structure or ROI in a more robust manner. As a feature of the highest activity least affected by the presence of outliers, the median was computed on the upper 10% of the SUV distribution (i.e., the range between the 90^{th} percentile of SUV distribution and its last bin, corresponding to SUV_{max}). Thus, by definition, this parameter is statistically significant for the highest uptake and intrinsically

more robust than SUV_{max}, which can be an outlier instead. Being equivalent to the 95th value of the total SUV distribution, it is hereafter indicated as SUV_{95th}. To better understand the implications of SUV_{95th}, as an example, the integral distribution of the SUV values belonging to the left kidney of patient ID5 (b-PET/CT) is reported in blue in Fig. 4. Fig. 4 (a) evidences the subdivision of the distribution into deciles. Fig. 4 (b) highlights in green the last decile, the part of distribution considered to compute SUV_{95th}, pointed out in magenta, and the value of SUV_{max}, in red. As one can see, SUV_{max} represents an outlier for the distribution, contrarily to SUV_{95th}.

Fig. 4 Distribution of SUV values (b-PET/CT) related to the left kidney of patient ID5 (in blue) and its partition into deciles (a). The last decile (in green) considered to compute SUV_{95th} (in magenta), and SUV_{max} of the distribution (in red) (b).

Statistical Analysis

The differences in SUV_{95th} between b-PET/CT and m-PET/CT were assessed independently of the infusion protocol due to the small number of cases considered. To this purpose, the Kruskal-Wallis test, used to compare group medians, was performed on the upper 10% of the SUV distributions for each kidney. A comparison between SUV_{max} and SUV_{95th} was also performed. Statistical analysis was carried out with Matlab© (MathWorks, Natick, MA, USA). *p*-value < 0.001 was considered significant.

Results

Table 1 shows SUV_{max} and SUV_{95th} values (presented as mean ± standard deviation) obtained with 2 two mannitol infusion protocols, derived from both kidneys and referred to as b-PET/CT and m-PET/CT examinations.

Fig. 5 shows SUV_{max} and SUV_{95th} values for the right and left kidneys, respectively, computed on the complete dataset and referring to b-PET/CT (blue) and m-PET/CT (red).

Fig. 5 SUV_{max} (a) and SUV_{95th} (b) values of right kidneys (RK). SUV_{max} (c) and SUV_{95th} (d) values of left kidneys (LK). Values referring to baseline examinations (b-PET/CT) are reported in blue, while those referring to follow-up scans after mannitol infusion (m-PET/CT) in red. A-patient samples are shown with a dashed line (ID1-ID3) and B-patient samples with a solid line (ID4-ID9).

A-patient samples are shown with a dashed line, B-patient samples with a solid line. In three A-infusion patients (ID1, ID2 and ID3), SUV_{max} globally increased during m-PET/CT for both right (Fig. 5 (a)) and left (Fig. 5 (c)) kidneys. Patient ID1 showed similar SUV_{max} value for both kidneys. With regard to six B-infusion patients (ID4 to ID9), SUV_{max} follow-up values were lower than those of baseline in both kidneys, with the exception of ID8 for both right and left kidneys, for which values remain unchanged.

These results were only partly confirmed by SUV_{95th}. Actually, SUV_{95th} showed that ID1, the A-infusion patient with similar SUV_{max} values for both kidneys, was characterized by a lower uptake at the follow-up scan. Conversely, follow-up SUV_{95th} values of B-infusion patients were always lower than corresponding baseline values. This also occurred for patient ID8, who showed slightly increased SUV_{max} values for both kidneys. The Kruskal-Wallis test computed for each kidney revealed that differences between baseline and follow-up SUV_{95th} values were significant (p-value <0.001).

Discussion

Dosimetry studies have shown that organs such as kidneys and lacrimal and salivary glands exhibit tracer accumulation, which may limit the use of radiolabelled PSMA ligands [12]. We recently demonstrated the potentially protective effect of mannitol to reduce renal uptake of

PSMA and thus lower the absorbed dose to the kidneys [6]. However, the results were obtained using the SUV_{max} parameter and further dosimetric analyses were needed to confirm these findings [6].

SUV_{max} is a commonly used parameter in clinical practice and has several attractive features. It reflects the most metabolically active part of the region considered or the part with the highest expression [13], which, however, may not be the most clinically significant [14]. SUV_{max} is easily measured and is only slightly affected by partial-volume effects. Conversely, it is highly susceptible to unpredictable noise-derived variations, as described by Soret et al [15]. For the same reason, the use of other SUV parameters, such as mean (SUV_{mean}) and peak (SUV_{peak}) values derived as the mean value from the isocontour based on SUV_{max} [16], can also lead to an under- or overestimation of the uptake. In fact, 40% of SUV_{max} is usually considered as significant [17], a choice that appears objective and reliable at first glance. However, its reliability has never been proved. One of the drawbacks of this approach is that the percentage of SUV values considered for the SUV_{peak} measure, depending on the SUV_{max}, is more strongly affected by the amount of image noise. Moreover, regardless of the segmentation method adopted, the SUV_{mean}, being dependent on the definition of the ROI, is less reproducible than SUV_{max}, which is an observer-independent parameter [18, 19].

The SUV_{95th} implemented in the present work overcomes the vulnerability of SUV_{max}, which represents a single-pixel measurement, and is much less affected by noise. This is because it includes a significant part of the upper value distribution by taking into consideration its median value. Besides the specific application shown in this work, SUV_{95th} also overcomes the general limits of both SUV_{mean}, usually conditioned by partial volume effect and segmentation and thus prone to intra- and inter-observer variability, and SUV_{peak}, commonly performed through the isocontour based on the SUV_{max}. More importantly, SUV_{95th} maintains a clinically meaningful value by representing the highest PET activity in a more robust way. It is worth remarking that it requires no further data, since it can be easily

calculated starting from SUV value distributions coming from vendor software, used to compute SUV_{max}, and available in standard PET examinations.

In the present study, the results obtained with SUV_{95th} improved and statistically reinforced those obtained with SUV_{max}, also confirming that mannitol B-infusion protocol can safely reduce PSMA renal uptake. SUV_{95th} values referring to baseline and follow-up examinations differed significantly, even in the patients (ID1 and ID8) with similar baseline and follow-up SUV_{max} values. Of note, SUV_{95th} values obtained for ID8, one of the 6 B-infusion patients, strengthen the effectiveness of the B-infusion protocol as the best administration scheme to reduce renal uptake. Indeed, the values obtained with SUV_{95th} consistently showed that the short mannitol infusion of the B-infusion scheme (patients ID4 – ID9) led to a reduction in kidney uptake highlighted by m-PET/CT.

Although we are aware that the small case series represents a limitation of the present work, our findings on SUV_{95th} are anyway more reliable than those achieved with SUV_{max}. Further studies are now needed to confirm the clinical data so that proposed workflow can be implemented into clinical practice. Furthermore, as a future goal, SUV_{95th} will be also adopted to evaluate the role of mannitol in sparing the renal absorbed dose in therapy with new agents.

The new metric should be also tested to evaluate the therapeutic response of tumours, usually more severely affected by the partial volume effect. Optimal cut-off values based on SUV_{max} are often proposed in the literature as surrogate predictive biomarkers due to the failure of standardized criteria for the evaluation of tumour response to therapy. In our opinion, the methodological approach presented in the present study could lead to a more reliable assessment of clinical outcomes and response evaluation.

Conclusion

Our study underlines the advantages of SUV_{95th} over SUV_{max}. SUV_{95th}, derived as the median value of a distribution, is less affected by the presence of outliers than SUV_{max}. The

reliability of this parameter is promising and deserves to be proved on much larger datasets and different clinical settings. The results presented support the use of mannitol infusion before PSMA-PET/CT or radioligand therapy with 177Lu / 225Ac to reduce the adsorbed dose to the kidneys.

Acknowledgements

The authors would like to thank Filippo Piccinini for his help with data collection during the starting stage of this study.

Funding

This research was partially supported by the Italian Ministry of Health (grant RF-2016-02364230), and by the Italian Association for Cancer Research (AIRC), (grant IG 20476).

Authors' contributions

Study concept and design: AS, AB, SB.

Provision of study materials or patients: FM, AS, EM.

Collection and assembly of data: FM.

Radiopharmaceutical synthesis and quality control: VDI.

Diagnostic imaging: FM, PC.

Analysis and interpretation of data: SB, AB, AS.

Drafting of manuscript: SB.

Critical revision of the manuscript for important intellectual content: GP, AB, FM, AS.

All authors read and approved the final manuscript for submssion.

Ethical approval

The protocol was approved by the Ethics Committee of Area Vasta Romagna and by the competent Italian regulatory authorities. The study was performed in accordance with the principles of the Declaration of Helsinki and Good Clinical Practice.

Informed consent

All patients gave their written informed consent.

Conflicts of interest

The authors declare that they have no conflict of interest.

References

1. Afshar-Oromieh A, Avtzi E, Giesel FL, et al. (2015) The diagnostic value of PET/CT imaging with the 68 Ga-labelled PSMA ligand HBED-CC in the diagnosis of recurrent prostate cancer. Eur J Nucl Med Mol Imaging 42(2):197-209.
2. Han S, Woo S, Kim YJ, Suh CH (2018) Impact of 68 Ga-PSMA PET on the Management of Patients with Prostate Cancer: A Systematic Review and Meta-analysis. Eur Urol 74(2):179-90.
3. Afshar-Oromieh A, Zechmann CM, Malcher A, et al. (2014) Comparison of PET imaging with a 68 Ga-labelled PSMA ligand and 18 F-choline-based PET/CT for the diagnosis of recurrent prostate cancer. Eur J Nucl Med Mol Imaging 41(1):11-20.
4. Mannweiler S, Amersdorfer P, Trajanoski S, Terrett JA, King D, Mehes G (2009) Heterogeneity of prostate-specific membrane antigen (PSMA) expression in prostate carcinoma with distant metastasis. Pathol Oncol Res 15(2):167-72.
5. Baccala A, Sercia L, Li J, Heston W, Zhou M (2007) Expression of prostate-specific membrane antigen in tumor-associated neovasculature of renal neoplasms. Urology 70(2):385-90.
6. Matteucci F, Mezzenga E, Caroli P, et al. (2017) Reduction of 68Ga-PSMA renal uptake with mannitol infusion: preliminary results. Eur J Nucl Med Mol Imaging 44(13):2189-94.
7. Sarnelli A, Belli ML, Di Iorio V, et al. (2019) Dosimetry of 177Lu-PSMA-617 after Mannitol Infusion and Glutamate. Molecules 24(3):621
8. Schneider CA, Rasband WS, Eliceiri KW (2012) NIH Image to ImageJ: 25 years of image analysis. Nature methods 9(7):671.
9. Bolte S, Cordelieres FP (2006) A guided tour into subcellular colocalization analysis in light microscopy. J Microsc 224(3):213-32.

10. Ollion J, Cochennec J, Loll F, Escude C, Boudier T (2013) TANGO: a generic tool for high-throughput 3D image analysis for studying nuclear organization. Bioinformatics 29(14):1840-1.
11. Schwertman NC, Owens MA, Adnan R (2004) A simple more general boxplot method for identifying outliers. Comput Stat Data Anal 47(1):165-74.
12. Okamoto S, Thieme A, Allmann J, et al. (2017) Radiation dosimetry for 177Lu-PSMA I&T in metastatic castration-resistant prostate cancer: absorbed dose in normal organs and tumor lesions. J Nucl Med 58(3):445-50.
13. Hohberg M, Kobe C, Täger P, et al. (2019) Combined Early and Late [68 Ga] PSMA-HBED-CC PET Scans Improve Lesion Detectability in Biochemical Recurrence of Prostate Cancer with Low PSA Levels. Mol Imaging Biol 21(3): 558-566.
14. Lodge MA, Chaudhry MA, Wahl RL (2012) Noise considerations for PET quantification using maximum and peak standardized uptake value. J Nucl Med 53(7):1041.
15. Soret M, Bacharach SL, Buvat I (2007) Partial-volume effect in PET tumor imaging. J Nucl Med 48(6):932.
16. Ziai P, Hayeri MR, Salei A, et al. (2016) Role of optimal quantification of FDG PET imaging in the clinical practice of radiology. Radiographics 36(2):481-96.
17. Kang SY, Cheon GJ, Lee M, et al. (2017) Prediction of recurrence by preoperative intratumoral FDG uptake heterogeneity in endometrioid endometrial cancer. Transl Oncol 10(2):178-83.
18. Adams MC, Turkington TG, Wilson JM, Wong TZ (2010) A systematic review of the factors affecting accuracy of SUV measurements. Am J Roentgenol 195(2):310-20.
19. Lim RS, Ramdave S, Beech P, et al. (2016) Utility of SUV max on 18 F-FDG PET in detecting cervical nodal metastases. Cancer Imaging 16(1):39.

Table 1 SUV_{max} and SUV_{95th} values from b-PET/CT and m-PET/CT in both kidneys (right and left) of patients undergoing different administration schemes (A-infusion, 3 patients, and B-infusion, 6 patients).

		Right kidney		Left kidney	
SUV index	**Administration protocol**	**b-PET/CT**	**m-PET/CT**	**b-PET/CT**	**m-PET/CT**
SUV_{max}	A-infusion	42.9 ± 4.6	48.7 ± 8.3	44.6 ± 7.8	48.1 ± 10.3
	B-infusion	61.0 ± 10.8	46.2 ± 10.5	59.0 ± 15.8	45.8 ± 12.0
SUV_{95th}	A-infusion	31.9 ± 1.7	36.1 ± 11.1	31.8 ± 3.0	36.3 ± 12.2
	B-infusion	41.2 ± 8.1	30.9 ± 9.7	40.3 ± 6.1	29.2 ± 9.4

Fig. 1 Flowchart of the computer-assisted 3D kidney segmentation.

ROI, region of interest

Fig.2 Example of kidney segmentation (a). The procedure starts with manually outlining the kidney (b) and the selection of the window/level (W/L). The resulting image (c) is used for the object detection (d). The last step involves the filling of the object detected (e).

ROI, region of interest

Fig. 3 3D visualization of the kidneys. Regions with lower uptake such as the renal pelvis were almost discarded during the processing phase. To facilitate subsequent analysis and 3D measurements, results of the object detection were post-processed through in-house developed ImageJ Macro softward.

Fig. 4 Distribution of SUV values (b-PET/CT) related to the left kidney of patient ID5 (in blue) and its partition into deciles (a). The last decile (in green) considered to compute SUV_{95th} (in magenta), and SUV_{max} of the distribution (in red) (b).

Fig. 5 SUV_{max} (a) and SUV_{95th} (b) values of right kidneys (RK). SUV_{max} (c) and SUV_{95th} (d) values of left kidneys (LK). Values referring to baseline examinations (b-PET/CT) are reported in blue, while those referring to follow-up scans after mannitol infusion (m-PET/CT) in red. A-patient samples are shown with a dashed line (ID1-ID3) and B-patient samples with a solid line (ID4-ID9).

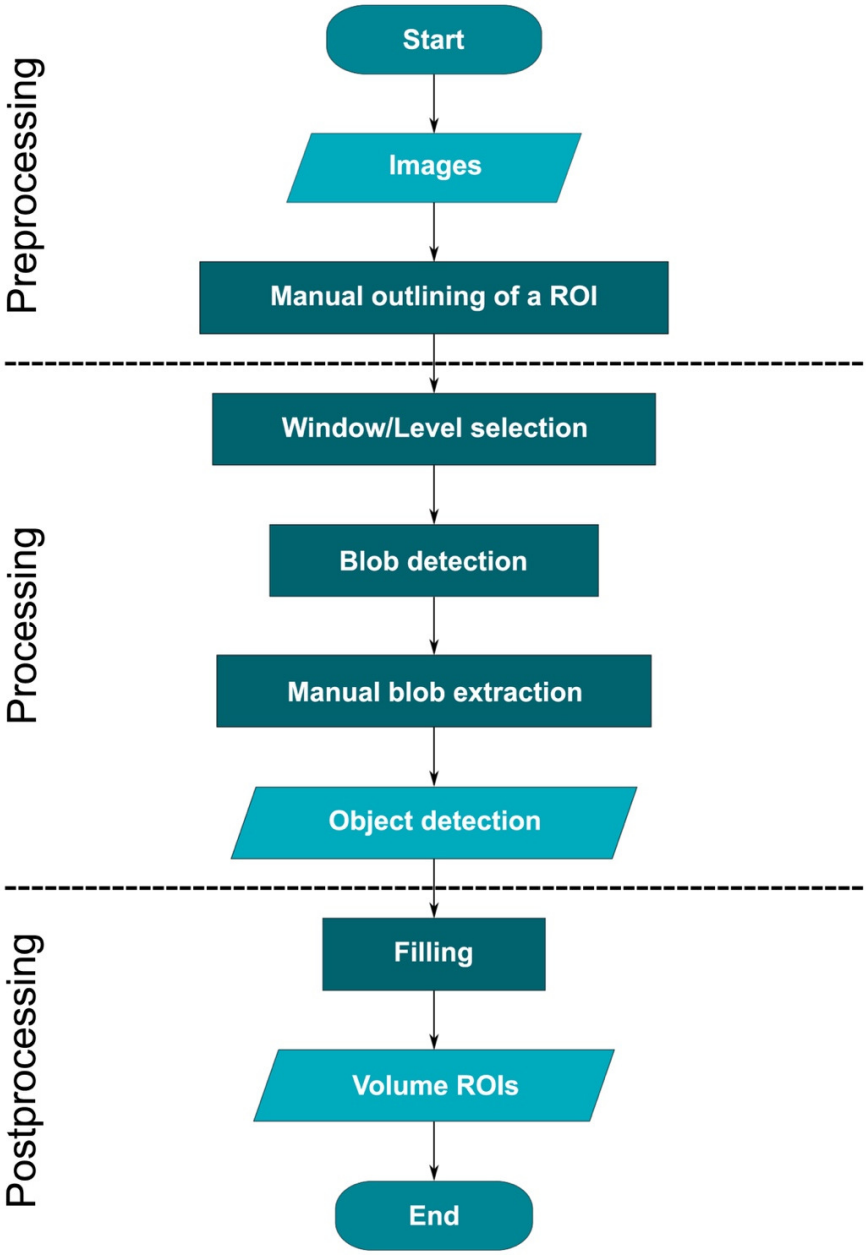

Fig. 1 Flowchart of the computer-assisted 3D kidney segmentation. ROI, region of interest

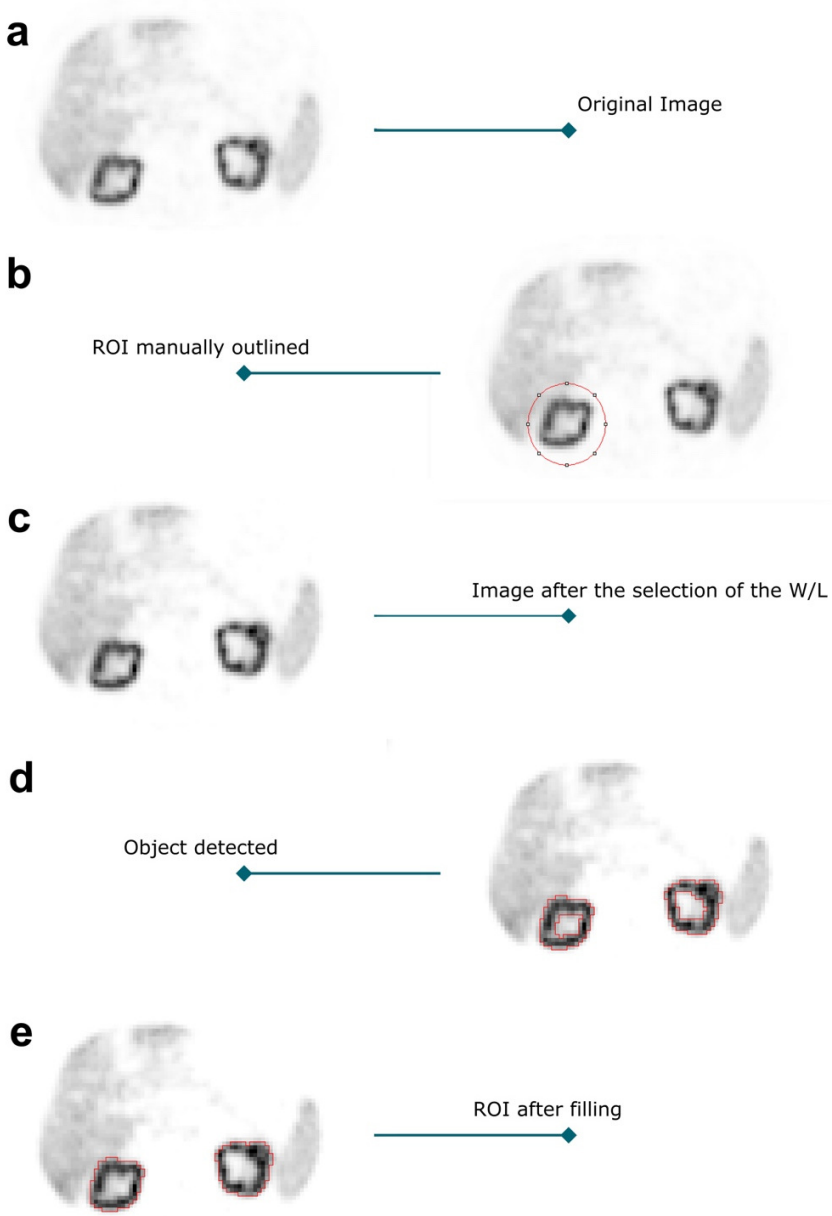

Fig.2 **a** - **e** Example of kidney segmentation. The procedure starts with **b** manually outlining the kidney and **c** the selection of the window/level (W/L). **d** The resulting image is used for the object detection. **e** The last step involves the filling of the object detected.

ROI, region of interest

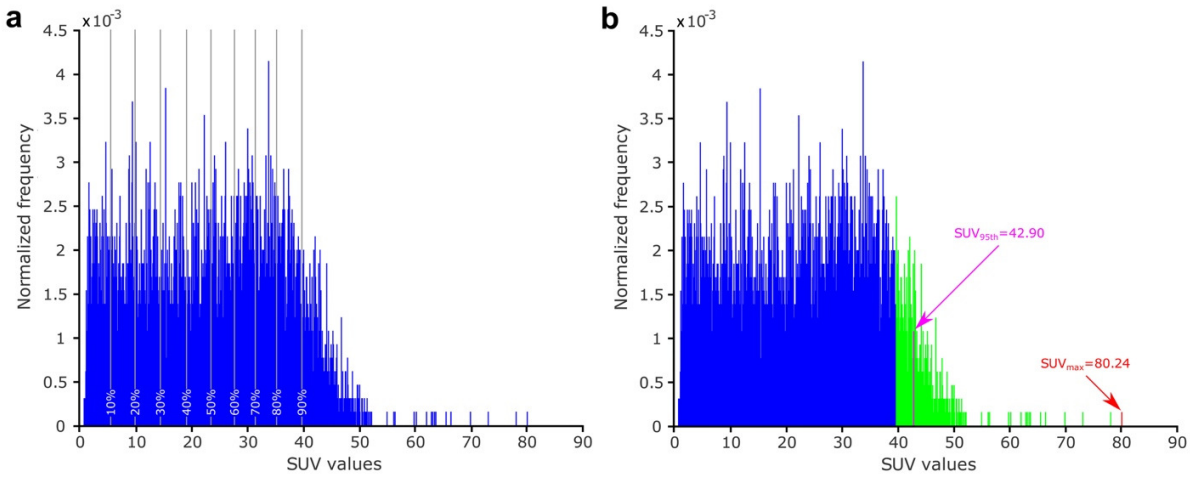

Fig. 4 **a** Distribution of SUV values (b-PET/CT) related to the left kidney of patient ID5 (in blue) and its partition into deciles. **b** The last decile (in green) considered to compute SUV_{95th} (in magenta), and SUV_{max} of the distribution (in red).

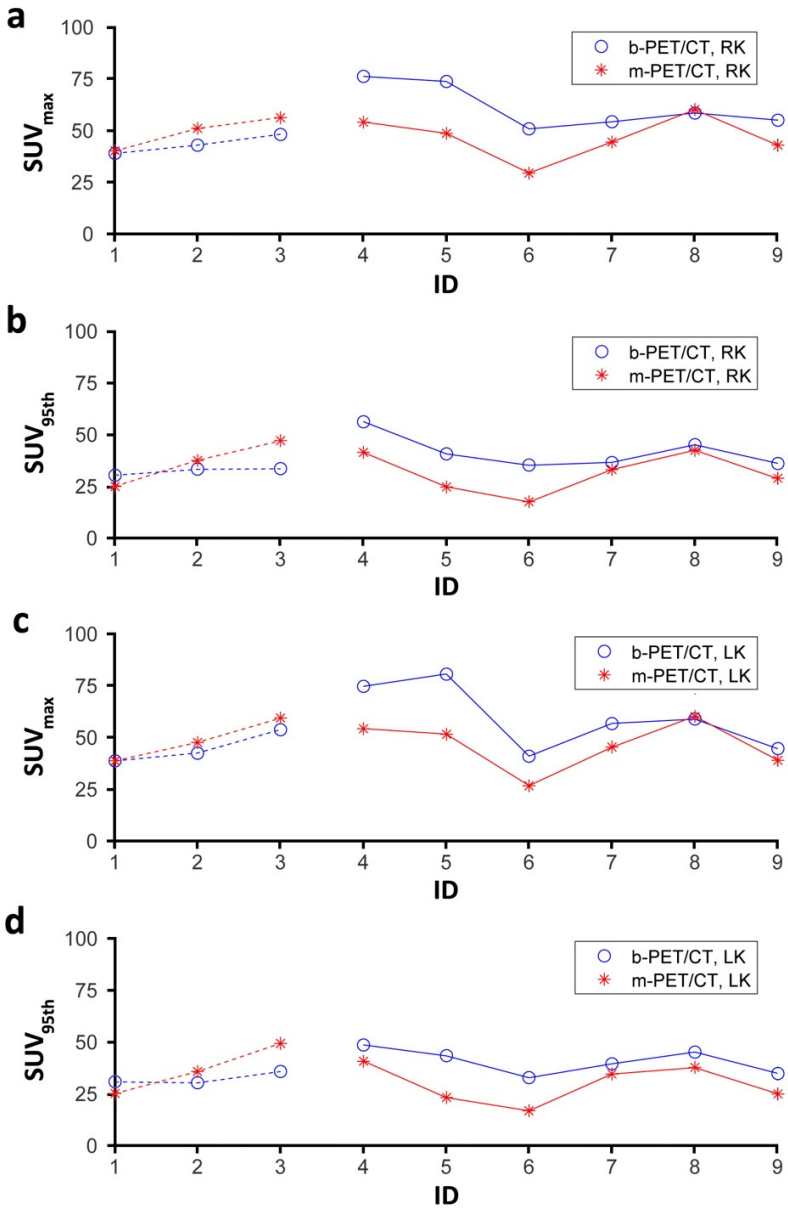

Fig. 5 **a** SUV_{max} and **b** SUV_{95th} values of right kidneys (RK). **c** SUV_{max} and **d** SUV_{95th} values of left kidneys (LK). Values referring to baseline examinations (b-PET/CT) are reported in blue, while those referring to follow-up scans after mannitol infusion (m-PET/CT) in red. A-patient samples are shown with a dashed line (ID1-ID3) and B-patient samples with a solid line (ID4-ID9).